BIOCHEMISTRY
including biophysical chemistry & molecular biology

Article

pubs.acs.org/biochemistry

G503 Is Obligatory for Coupling of Regulatory Domains in NCX Proteins

Moshe Giladi,[†] Itay Friedberg,[†] Xianyang Fang,[‡] Reuben Hiller,[†] Yun-Xing Wang,[‡] and Daniel Khananshvili*,[†]

[†]Department of Physiology and Pharmacology, Sackler School of Medicine, Tel-Aviv University, Ramat-Aviv 69978, Israel

[‡]Protein−Nucleic Acid Interaction Section, Structural Biophysics Laboratory, National Cancer Institute at Frederick, National Institutes of Health, Frederick, Maryland 21702, United States

Supporting Information

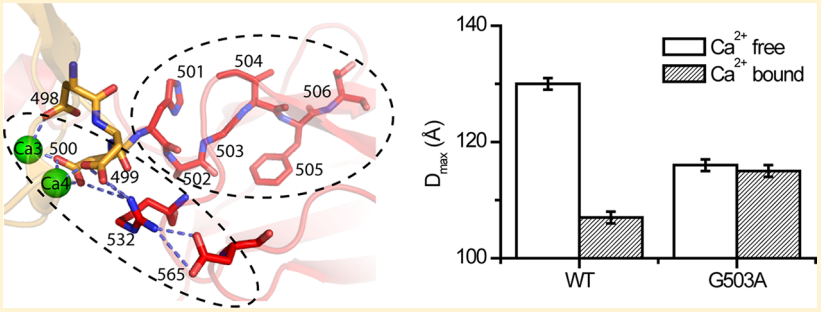

ABSTRACT: In multidomain proteins, interdomain linkers allow an efficient transfer of regulatory information, although it is unclear how the information encoded in the linker structure coins dynamic coupling. Allosteric regulation of NCX proteins involves Ca^{2+}-driven tethering of regulatory CBD1 and CBD2 (through a salt bridge network) accompanied by alignment of CBDs and Ca^{2+} occlusion at the interface of the two CBDs. Here we investigated "alanine-walk" substitutions in the CBD1−CBD2 linker (501-HAGIFT-506) and found that among all linker residues, only G503 is obligatory for Ca^{2+}-induced reorientations of CBDs and slow dissociation of occluded Ca^{2+}. Moreover, swapping between positions A502 and G503 in the CBD1−CBD2 linker results in a complete loss of slow dissociation of occluded Ca^{2+}, meaning that dynamic coupling of CBDs requires an exact pose of glycine at position 503. Therefore, accumulating data revealed that position 503 occupied by glycine is absolutely required for Ca^{2+}-driven tethering of CBDs, which in turn limits the linker's flexibility and, thus, restricts CBD movements. Because G503 is extremely well conserved in eukaryotic NCX proteins, the information encoded in G503 is essential for dynamic coupling of the two-domain CBD tandem and, thus, for propagation of the allosteric signal.

Linkers of different sizes connect multiple domains, thus allowing an efficient transfer of information between separate domains.[1−3] Although it has been known for a while that the length and sequence of the linker control allosteric signal transmission in multidomain proteins,[4−6] the information encoded in the linker's sequence is perhaps far more important than it was originally thought.[6,7] For example, recent work suggests that linkers encode successive conformational transitions in managing allosteric signal transfer and, therefore, behave as the "vehicle".[5−7]

The Na^+/Ca^{2+} exchanger proteins (NCX1−3) extrude Ca^{2+} from the cell[8−10] and are allosterically regulated by the binding of Ca^{2+} to regulatory domains, CBD1 and CBD2, which form a "head-to-tail" tandem (CBD12) through a short linker.[11,12] CBD1 contains a primary Ca^{2+} sensor (Ca3 and Ca4 sites), located next to the CBD1−CBD2 linker, whereas CBD2 contains a splice variant segment, which arises from the combination of six small exons.[12−16] It remains unclear how in NCX proteins the information is primarily decoded upon Ca^{2+} binding to Ca3 and Ca4 sites and further transferred to distantly located ion transport domains.[14−18]

Several lines of evidence suggest that Ca^{2+}-dependent allosteric regulation of NCX involves synergistic interactions between CBDs,[19−22,25] whereas CBD2 interacts with CBD1 to increase Ca^{2+} affinity at the Ca3 and Ca4 sites.[20,23,24] Synergistic interactions between CBDs are most prominently manifested as slow dissociation ($k_s \sim 0.5\ s^{-1}$) of occluded Ca^{2+} from Ca3 and Ca4 sites of CBD12.[19,23,24,29] This phenomenon is associated with slow reorientation of CBDs either in the isolated CBD12 or in full-size NCX,[20] thereby representing slow inactivation of intact NCX in the cellular system.[26−28]

In conjunction with X-ray crystallography, stopped-flow kinetics, and SAXS analyses of CBD12 mutants (of the brain splice variant), we demonstrated that binding of Ca^{2+} to Ca3 and Ca4 sites is associated with interdomain tethering (Figure

Received: June 28, 2012
Revised: August 26, 2012

   dx.doi.org/10.1021/bi300739z | *Biochemistry* XXXX, XXX, XXX−XXX

1) and slow dissociation of occluded Ca^{2+}.[29] This interdomain network involves amino acids from both CBD1 and CBD2,

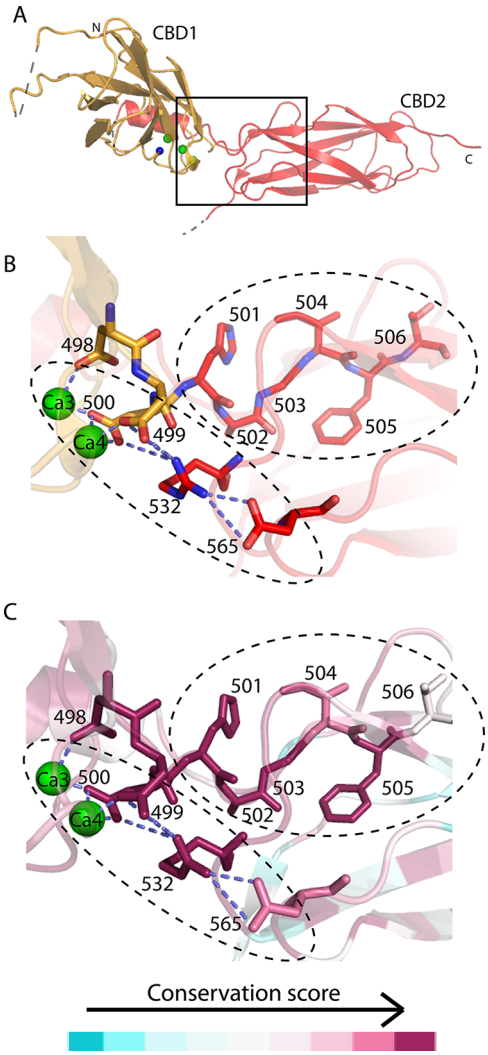

Figure 1. Structure of the CBD12 tandem. (A) Overall structure of CBD12-E454K (Protein Data Bank entry 3US9). CBD1 and CBD2 are colored orange and red, respectively. Dashed lines represent chain breaks. Green and blue spheres depict Ca^{2+} ions and water molecules, respectively. The rectangle frames a close-up as depicted in panels B and C. Dashed ellipses circle the linker residues (501–506) and the salt bridge network. In panel C, the residues are colored according to their conservation score as calculated by Consurf.

whereas the buried R532 located in CBD2 tethers D565 from CBD2 and D499 and D500 from CBD1. Most importantly, the bifurcated salt bridges between R532 and D499 and D500 support Ca^{2+} coordination at the Ca3 and Ca4 sites and are obligatory for slow Ca^{2+} dissociation and Ca^{2+}-induced alignment of CBDs.[29] A similar network of interdomain salt bridges was found in *Drosophila* (CALX) CBD12.[30] A recent NMR study revealed that binding of Ca^{2+} to CBD1 rigidifies the linker's flexibility and CBD movements.[25] To further elucidate the structural determinants governing dynamic coupling of CBDs, we analyzed here how single-point mutations in the linker (501-HAGIFT-506) affect Ca^{2+} off rates and Ca^{2+}-induced alignment of CBDs by using stopped-flow and SAXS techniques.

Sequential (biphasic) dissociation of two Ca^{2+} ions from the Ca3 and Ca4 sites of CBD12 consists of a fast ($k_f \sim 5\ s^{-1}$) and a slow ($k_s \sim 0.5\ s^{-1}$) phase, whereas the slow rate constant (k_s) represents a dissociation of the second (occluded) Ca^{2+} from CBD12.[19,23] We previously demonstrated that combining X-ray, SAXS, and stopped-flow techniques is very instrumental in characterizing Ca^{2+}-dependent interactions in CBD12.[19,23,29] For example, mutations in the salt bridge interfacial residues abort Ca^{2+} occlusion, exhibiting monophasic off rates with a 20–50-fold acceleration of k_s values.[29] Because slow dissociation of Ca^{2+} is observed in CBD12 (but not in isolated CBD1 or CBD2) and the elongation of the CBD1–CBD2 linker results in a loss of slow dissociation of occluded Ca^{2+},[19,23,29] we used these hallmarks for evaluating synergistic interactions between CBDs. We examined here single-point mutations in the CBD1–CBD2 linker for their effects on slow Ca^{2+} dissociation in the isolated preparations of CBD12.

EXPERIMENTAL PROCEDURES

Overexpression and Purification of CBD12 Proteins. The DNA constructs of CBD12 (encoding residues 371–657) of canine NCX1 (accession code P23685; AD-splice variant) were cloned into the pET23b vector and expressed in *Escherichia coli* Rosetta2 (DE3) competent cells (Novagen), as described previously.[18,19] Mutations were introduced by QuickChange mutagenesis (Stratagene) and confirmed by sequencing. Overexpressed proteins were purified on Ni beads (>90% purity, judged by sodium dodecyl sulfate–polyacrylamide gel electrophoresis). Proteins were concentrated and decalcified by addition of 10 mM EDTA. To remove EDTA, the protein preparations were washed with decalcified buffer using an Ultracel-3k concentrator to reach an EDTA concentration of <1 nM.[23,24]

Conservation Analysis of CBD12. The Ensembl server[36] was used to search for canine NCX orthologs. These sequences were used to generate a multiple-sequence alignment using Clustalw.[37] The resulting alignment was used as input for Consurf,[38] to calculate a conservation score for each residue.

Equilibrium $^{45}Ca^{2+}$ Binding Assay. The equilibrium binding of $^{45}Ca^{2+}$ to proteins was measured as the protein-bound radioactivity retained after ultrafiltration.[18,19,23,24] The assay medium (1.5 mL) containing 7–15 μM protein with 100 mM KCl and 10 mM Tris-HCl (pH 7.2) (TK buffer) was placed in the upper chamber of the Ultracel-3k concentrator, and the assay was performed as previously outlined.[18,19,23,24] The $[Ca^{2+}]_{free}$ fraction was measured as a/b, where a represents the radioactivity of the ultrafiltate and b represents the radioactivity in the upper chamber; thus, $[Ca^{2+}]_{free} = [Ca^{2+}]_{tot}(a/b)$. The level of bound Ca^{2+} is calculated as $[Ca^{2+}\text{-CBD}] = [Ca^{2+}]_{tot} - [Ca^{2+}]_{free}$ and binding stoichiometry as $[Ca^{2+}\text{-CBD}]/[CBD]$. The $^{45}Ca^{2+}$ titration curves of CBD12 were fit to Adair equations with a predefined number of binding sites according to the observed maximal binding capacity using GraFit (Erithacus Software, Ltd.).[18,19,23,24] $[Ca^{2+}]_{residual}$ of decalcified buffer was measured with Fluo-3.[18] All other procedures were described previously.[18]

Stopped-Flow Experiments. The stopped-flow assays were conducted with a three-syringe, two-mixer SFM-3 machine (Bio-Logic) as outlined previously.[18,19,23,24,29] The data were analyzed with Bio-Kine 32 version 4.45 (Bio-Logic). Briefly, in the stopped-flow experiments, the dissociation of Ca^{2+} from proteins was monitored with the fluorescent Ca^{2+} chelator, Quin-2, as previously described;[18] 150 μL of 10 μM

dx.doi.org/10.1021/bi300739z | *Biochemistry* XXXX, XXX, XXX–XXX

protein (pre-equilibrated with $[Ca^{2+}]_{free}$ values of 5−10 μM) was mixed with 150 μL of 200 μM Quin-2 in TK buffer. Following mixing, $[Ca^{2+}]_{free}$ decreases abruptly (<2 ms) and Ca^{2+} dissociates from the protein, resulting in its binding to Quin-2, accompanied by an increase in fluorescence. Because the binding of Ca^{2+} to Quin-2 is nearly a diffusion-controlled reaction, the rate of increase in fluorescence reflects the kinetics of dissociation of Ca^{2+} from the examined protein.[18] The dead time is ~4 ms, allowing one to measure rate constants up to ~200 s^{-1}. Thus, only the off rates of high-affinity sites of CBD preparations are observed.

SAXS Data Collection, Analysis, and Bead Model Reconstruction. Data were recorded at the Advanced Photon Source. The energy of the X-ray beam was 12 keV (wavelength λ = 1.033 Å), and the distance from the sample to detector (PILATUS 2M, Dectris Ltd.) was 2 m, covering a scattering vector range ($q = 4\pi \sin\theta/\lambda$) from 0.007 to 0.66 $Å^{-1}$, as determined by the scattering profile of silver behenate. Twenty frames of two-dimensional (2D) images were recorded for each buffer or sample using a flow cell, with an exposure time of 5 s for each frame to improve the signal:noise ratio and with a sleep time of 1 s between each frame to reduce radiation damage. The 2D images were reduced to one-dimensional scattering profiles using the Matlab scripts on site. The scattering profile of a sample solute was calculated by subtracting the buffer contribution from the sample−buffer profile using PRIMUS.[39] The experimental radius of gyration (R_g) and the forward scattering intensity [$I(0)$] were calculated from data at low q values in the range of $qR_g < 1.3$, using the Guinier approximation: $\ln I(q) \approx \ln[I(0)] - R_g^2 q^2/3$. The pair distance distribution function (PDDF), $p(r)$, and the maximal dimension of the protein, D_{max}, in real space were calculated with the indirect Fourier transform using GNOM.[40] To avoid underestimation of the molecular dimension and consequent distortion in low-resolution structural reconstruction, the parameter D_{max}, the upper end of distance r, was chosen such that the resulting PDDF has a short, near-zero tail at large r values. Ab initio shape reconstructions were performed with DAMMIN,[41] using scattering data of the q range between 0.02 and 0.30 $Å^{-1}$; 32 independent DAMMIN calculations for each construct were performed. The resulting bead models were subjected to averaging by DAMAVER[42] where the normalized spatial discrepancy (NSD) values between each pair of models were computed. The model with the lowest average NSD with respect to the rest of models was chosen as the reference model. The remaining models were superimposed onto the reference model using SUPCOMB[43] except that possible outliers identified by NSD criteria were discarded. The dummy atoms of these superimposed models were remapped onto a densely packed grid of atoms with each grid point marked with its occupancy factor. The grids with non-zero occupancies were chosen to generate a final consensus model with a volume equal to the average excluded volume of all the models. The final models were filtered using DAMFILT.

RESULTS

In this work, the length of the CBD1−CBD2 linker was kept unchanged (as it is strictly conserved among NCX proteins), whereas residues 501−506 were systematically replaced with proline or alanine and subsequently analyzed for their effects on equilibrium Ca^{2+} binding and off rates. Substitutions H501A and A502P have no appreciable effect on Ca^{2+} binding titration curves (Figure 2A,C) or slow dissociation of Ca^{2+} (Figure 2B,D,F), suggesting that these two amino acids are not essential for synergistic interactions in CBD12. However, G503P, I504P, F505P, and T506P mutants exhibit 3−10-fold lower affinity for Ca^{2+} binding at Ca3 and Ca4 sites, with a reduced overall capacity for Ca^{2+} binding as compared with that of CBD12-WT (Figure 2A,C). All proline substitutions in the C-terminus of the linker (residues 503−506) lack the capacity for slow dissociation of Ca^{2+} (Figure 2B,D,F), implying that proline-attributed conformational constraints may prevent Ca^{2+} occlusion at Ca3 and Ca4 sites. An alternative possibility is that proline substitutions result in steric perturbations of the β-strands in CBD2, without playing a specific role in aligning CBDs.

For further resolution of the linker's role in Ca^{2+} occlusion, residues 503−506 were replaced with alanine. Notably, the

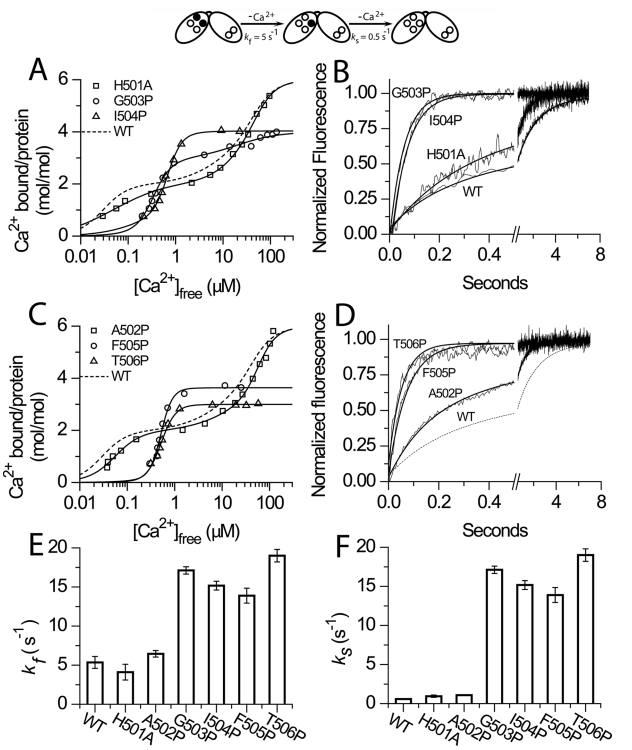

Figure 2. Effect of proline substitutions in the CBD12 linker on Ca^{2+} binding and off rates. (A) $^{45}Ca^{2+}$ titration curves of CBD12-WT and mutants CBD12-H501A, CBD12-G503P, and CBD12-I504P. (B) Representative traces of the kinetics of dissociation of Ca^{2+} from CBD12-H501A, CBD12-G503P, and CBD12-I504P. The representative traces of CBD12-WT and CBD12-H501A were fit to a double-exponential curve with a k_f of 3.62 ± 0.02 s^{-1} and a k_s of 0.59 ± 0.001 s^{-1} for CBD12-WT and a k_f of 3.92 ± 0.03 s^{-1} and a k_s of 0.92 ± 0.004 s^{-1} for CBD12-H501A. The representative traces of CBD12-G503P and CBD12-I504P were fit to a single-exponential curve with k_f values of 17.17 ± 0.08 and 15.25 ± 0.07 s^{-1}, respectively. (C) $^{45}Ca^{2+}$ titration curves of mutants CBD12-A502P, CBD12-F505P, and CBD12-T506P. (D) Representative traces of the kinetics of dissociation of Ca^{2+} from CBD12-A502P, CBD12-F505P, and CBD12-T506P. The representative trace of CBD12-A502P was fit to a double-exponential curve with a k_f of 6.6 ± 0.05 s^{-1} and a k_s of 1.1 ± 0.003 s^{-1}. The data of CBD12-F505P and CBD12-T506P were fit to a single-exponential curve with k_f values of 13.7 ± 0.12 and 19.0 ± 0.15 s^{-1}, respectively. (E) The bars represent the mean ± SE of k_f values for CBD12-WT, CBD12-H501A, and proline-substituted residues 502−506 in CBD12 (n = 6). (F) The bars represent the mean ± SE of k_s values for CBD12-WT, CBD12-H501A, and Pro-substituted residues 502−506 in CBD12 (n = 6).

dx.doi.org/10.1021/bi300739z | Biochemistry XXXX, XXX, XXX−XXX

linker amino acid mutants I504A and T506A exhibit nearly "normal" Ca^{2+} binding (Figure 3A) and retain a slow phase for

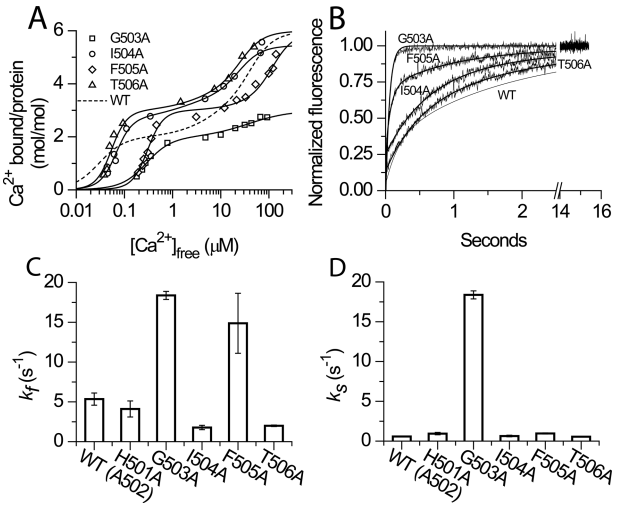

Figure 3. Kinetic and equilibrium properties of alanine substitutions of the linker residues (503−506). (A) $^{45}Ca^{2+}$ titration curves of CBD12-G503A, CBD12-I504A, CBD12-F505A, and CBD12-T506A. (B) Representative traces of the kinetics of dissociation of Ca^{2+} for CBD12-G503A, CBD12-I504A, CBD12-F505A, and CBD12-T506A. Because the rapid component of dissociation of Ca^{2+} from low-affinity sites was also observed,[18] these mutants were fit to a triple-exponential curve: k_r = 227.4 ± 11.4 s^{-1}, k_f = 1.70 ± 0.006 s^{-1}, and k_s = 0.58 ± 0.002 s^{-1} for CBD12-I504A, k_r = 131.3 ± 5.91 s^{-1}, k_f = 13.4 ± 0.15 s^{-1}, and k_s = 1.00 ± 0.005 s^{-1} for CBD12-F505A, and k_r = 159.9 ± 14.5 s^{-1}, k_f = 1.9 ± 0.008 s^{-1}, and k_s = 0.52 ± 0.001 s^{-1} for CBD12-T506A. The representative trace of CBD12-G503A was fit to a single-exponential curve with a k_f of 18.3 ± 0.10 s^{-1}. (C) The bars represent the mean ± SE of k_f values for CBD12-WT and alanine-substituted residues 501 and 503−506 (n = 6). (D) The bars represent the mean ± SE of k_s values for CBD12-WT and Ala-substituted residues 501 and 503−506 (n = 6). For CBD12-G503A, k_f and k_s are identical because no slow component is observed.

Ca^{2+} dissociation (Figure 3B,D). Mutant F505A shows altered binding affinity but retains the binding capacity and slow phase of dissociation. In contrast, the CBD12-G503A mutant exhibits a Ca^{2+} titration curve typical of CBD1-WT (Figure 3A and Figure S1 and Table S1 of the Supporting Information). Most probably, the Ca^{2+} binding capacity of CBD2 is altered in CBD12-G503A. Moreover, CBD12-G503A lacks a slow phase for Ca^{2+} dissociation, while showing typical off rates of CBD1-WT (Figure 3B,D). Thus, the G503 mutation in CBD12 concomitantly alters Ca^{2+} occlusion at Ca3 and Ca4 sites of CBD1 and Ca^{2+} binding capacity at CBD2. An alternative interpretation is that the G503 mutation alters two low-affinity sites (Ca1 and Ca2) at CBD1. However, this interpretation is unlikely, because although CBD1 was crystallized without G503 and upstream residues, the structure shows ion coordination identical to that of CBD12 for all CBD1's sites.[30,32] Moreover, G503 participates in the β-strand interactions of CBD2.[31] Finally, the G555P mutation in CALX-CBD12 (corresponding to G503P in this study) resulted in intact capacity but reduced affinity.[30] Because the CBD2 domain does not bind Ca^{2+} in CALX,[30,31] it can be concluded that the CBD1 sites preserve their binding capacity. Thus, it is likely that the binding sites of CBD2 are affected by the mutation. Importantly, the global folding of either CBD1 or CBD2 remains unaltered in the G503 mutant, as revealed by SAXS data (see below). Table S1 of the Supporting Information describes the fitting parameters for Ca^{2+} binding obtained for different CBD12 mutants.

To investigate the possible consequences of the G503A mutation that may affect Ca^{2+}-induced alignment of CBDs, we monitored Ca^{2+}-dependent conformational transitions using SAXS techniques. The pair distance distribution function (PDDF) of CBD12-WT (Figure 4D) reveals a major conformational transition upon Ca^{2+} binding, with D_{max} values of 130 ± 1 and 107 ± 1 Å for the Ca^{2+}-free and Ca^{2+}-bound forms, respectively (Figure 4B,D). In sharp contrast, G503A (D_{max} = 116 ± 1 and 115 ± 1 Å for the Ca^{2+}-free and Ca^{2+}-bound forms, respectively) does not show Ca^{2+}-dependent reorientation (Figure 4A,B,F). Interestingly, the D_{max} values of CBD12-G503A are approximately an average value between the Ca^{2+}-bound and free D_{max} values of CBD12-WT. It is noteworthy that the overall shape of CBD12-G503A seems intact (Figure 4A), despite its reduced Ca^{2+} binding capacity, thus excluding the possibility of unfolding imposed by the G503A mutation. Therefore, the G503A mutant lacks both slow dissociation of occluded Ca^{2+} and Ca^{2+}-induced alignment of CBDs, meaning that the G503A mutant knocks out Ca^{2+}-driven local interactions at the two-domain interface.

Collectively, our data thus far indicate an important role for G503 in domain coupling. It may be argued that the position of this glycine residue is not important, and that its role results only from the flexibility provided to the linker; i.e., only the composition of the linker is important. To address this possibility, we have swapped positions between A502 and G503 (CBD12-GA). As in CBD12-G503A, this mutant exhibits monophasic dissociation kinetics with rate constants nearly identical to those of CBD1-WT (Figure 5). Thus, the exact position of G503 is essential for dynamic coupling of CBDs as reflected by the lack of Ca^{2+} occlusion in CBD12-GA. The amplitude values and rate constants of all the mutants analyzed by fitting the stopped-flow data to multiphasic kinetics are listed in Table S2 of the Supporting Information.

DISCUSSION

Recent evidence suggests that the CBD1−CBD2 interface controls Ca^{2+}-driven tethering of CBDs, which is associated with Ca^{2+} occlusion at the primary regulatory sensor (Ca3 and Ca4 sites) and with Ca^{2+}-dependent alignment of CBDs.[29] High-resolution X-ray structures of isolated CBD12, obtained from NCX1[29] and CALX,[30] clearly revealed that occupation of the Ca3 and Ca4 sites by two Ca^{2+} ions drives interdomain tethering of CBDs through the relay of the bifurcated salt bridge network. By analyzing CBD12 mutants with X-ray crystallography, SAXS, and stopped-flow techniques, we found that the amino acids involved in the interdomain salt bridge network (but not in Ca^{2+} ligation) are essential for performing slow dissociation of occluded Ca^{2+} and for Ca^{2+}-induced alignment of CBDs.[29] At this end, it was not clear if the linker encodes any specific structural information that may govern dynamic coupling of CBDs.

Our data reveal that among all amino acids in the CBD1−CBD2 linker, only the replacement of G503 can limit slow dissociation of occluded Ca^{2+} and Ca^{2+}-induced alignment of CBDs (Figures 3 and 4), thereby suggesting that the linker's G503 is essential for dynamic coupling of two regulatory domains. Moreover, the SAXS analysis shows that the CBD12-G503A mutant is unable to perform Ca^{2+}-dependent reorientation of CBDs, although the global folding of CBDs is unaltered (Figure 4). In CBD12-G503A, all four Ca^{2+} sites of

dx.doi.org/10.1021/bi300739z | Biochemistry XXXX, XXX, XXX−XXX

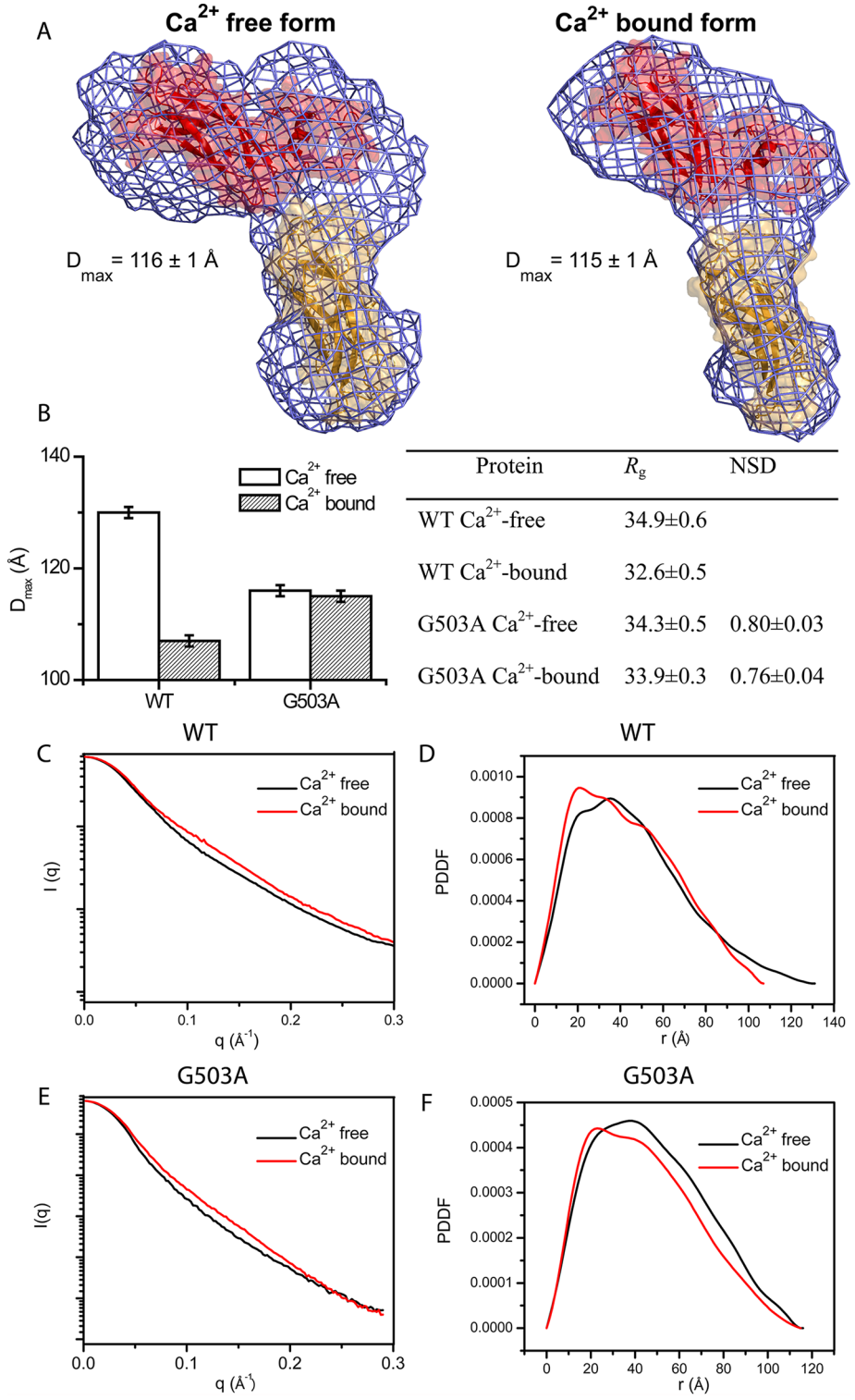

Figure 4. SAXS analysis of CBD12-WT and CBD12-G503A. (A) Bead model reconstruction of CBD12-G503A in the presence of 10 mM EDTA (left) or 10 mM $CaCl_2$ (right). (B) Overall SAXS parameters for CBD12-WT and CBD12-G503A. R_g, D_{max}, and NSD are the radius of gyration derived from Guinier plotting, the maximal interatomic dimension, and the normalized shape discrepancy for DAMMIN calculation, respectively. NSD scores are <0.8, indicating high convergence of the bead model calculations. (C–F) SAXS scattering curves of CBD12-WT (C) and CBD12-G503A (E) and pair distance distribution functions (PDDFs) of CBD12-WT (D) and CBD12-G503A (F) in the presence or absence of Ca^{2+}, as indicated.

CBD1 largely retain their wild-type affinity and capacity for Ca^{2+} binding (as compared with isolated CBD1), whereas the binding of Ca^{2+} to CBD2 seems to be altered. The Ca^{2+} binding properties of CBD12-G503A are dissimilar to those of the CBD12-7A mutant, in which seven alanine residues were inserted between H501 and A502.[19] In CBD12-7A, the elongated linker prevents Ca^{2+}-induced rigidification as the interface cannot form,[29] displaying properties similar to those

dx.doi.org/10.1021/bi300739z | Biochemistry XXXX, XXX, XXX–XXX

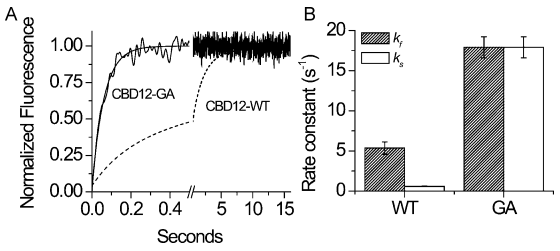

Figure 5. Effect of swapping positions A502 and G503. (A) Representative trace of Ca^{2+} dissociation kinetics for CBD12-GA fit to a single-exponential curve with a k_f of 16.2 ± 0.2 s^{-1}. (B) The bars represent the mean ± SE of k_f and k_s values for CBD12-WT and CBD12-GA (n = 6). For CBD12-GA, k_f and k_s are identical because no slow component is observed.

of a mixture of isolated CBD1 and CBD2. Interestingly, G555 of CALX1.1-CBD2 (which corresponds to G503 in NCX1-CBD12) is fully involved in the antiparallel β-strand interactions,[31] so it is possible that G503 interacts with the FG loop of NCX1-CBD2 to stabilize distantly located Ca^{2+}-binding sites of CBD2,[35] accounting for the reduced binding capacity of CBD12-G503A. These interactions could also be relevant for propagation of allosteric signals downstream to the membrane domains. Most importantly, the exact position of G503 is important for interdomain interactions as the CBD12-GA mutant lacks Ca^{2+} occlusion (Figure 5). This is supported by our conservation analysis, showing invariance in this residue position. Structurally, the dihedral φ and ψ angles of this residue in the crystal structure are only allowed for glycine, and any other residue in that specific position will require rotation around the Cα atom of this residue, resulting in steric clashes in the protein structure. This is true for G503 only in the context of CBD12. In the solution NMR structure of isolated CBD2 (Protein Data Bank entry 2FWU),[12] G503 is shown to take different orientations that are allowed for all residues.

Although the mutant F505A retains the slow phase of Ca^{2+} dissociation, it exhibits altered binding affinity at the high-affinity sites. According to the CBD12 tandem crystal structures,[29] this residue is completely buried in the hydrophobic core of the domain interface. As this residue forms a hydrophobic platform for many interface residues, any nonconservative substitution is expected to alter the binding properties of the tandem to some extent.

In general, interdomain motions can involve either large-scale structural rotations and translations of domains on time scales of 10^{-6} to 10^{-3} s or small-scale structural transitions of side chain−backbone dihedral angles in the range of 10^{-12} to 10^{-9} s, whereas segmental and loop movements can be between those ranges.[4−7] ^{15}N NMR relaxation data of CBD12 in the apo state indicate that two CBDs display nonlinear orientations on a 10^{-9} s time scale, whereas Ca^{2+} binding restricts the linker's flexibility to stabilize a more rigid conformation of CBDs without global changes in their reorientation.[25] Consistent with this, our data revealed that replacement of G503 with alanine or proline disconnects dynamic coupling between CBDs, accompanied by abortion of slow Ca^{2+} dissociation and Ca^{2+}-dependent alignment of CBDs. Interestingly, conformational transitions associated with dissociation of occluded Ca^{2+} and slow inactivation of intact NCX[19,20,23] are at least 10^3−10^4 times slower than typical rotational−translational movements observed for protein domains.[4−7] It is possible that allosteric signal propagation in NCX involves numerous conformational transitions with small energetic barriers to avoid dynamically unfavorable steps with a high energetic barrier. Obviously, the experimental testing of this possibility remains challenging.[5−7] On the basis of our findings, we suggest that glycine-dependent flexibility of short linkers may play a crucial role in the dynamic coupling of two-domain tandems in multidomain proteins.

Previous mutational studies revealed that both high-affinity sites (Ca3 and Ca4) of CBD1 contribute to Ca^{2+} occlusion, whereas after dissociation of the first Ca^{2+} ion, the second Ca^{2+} ion becomes occluded, most probably because of charge compensating interactions of the Ca3 and Ca4 sites with CBD2.[23,29] Accumulating data strongly support the notion that, on one hand, G503 coins the needed flexibility of the linker to direct Ca^{2+}-driven tethering of CBDs whereas, on the other hand, the relay of CBDs (upon Ca^{2+} binding) stabilizes stochastic oscillations of the linker to restrict CBD movements. We posit that after dissociation of the first Ca^{2+} ion, the interdomain salt bridges prevent complete unfolding of the Ca3 and Ca4 sites in CBD1 by electrostatic compensation, thereby allowing occlusion of the remaining ion. Following dissociation of the second Ca^{2+} ion, CBD1 binding sites may undergo further unfolding and, thus, prevent the interaction of R532 with CBD1. Because the two-domain interface is extremely well conserved among NCX variants,[29] the linker and salt bridge modules ascribe a two-in-one interface for dynamic coupling of CBDs. Obviously, the dynamic features of this common coupling unit are further modified by the alternative splicing segment located on CBD2.[16,23,29]

Because of large and rapid changes in the cytosolic Ca^{2+} concentration during the action potential, the Ca^{2+}-dependent allosteric activation of NCX is especially important in excitable tissues. For example, in cardiomyocytes, only ∼5% of the maximal NCX current is detected at resting $[Ca^{2+}]_i$ levels, whereas the increase in $[Ca^{2+}]_i$ to 1−2 μM recruits nearly 100% of the NCX-mediated current.[19] Studying the physiological contribution of Ca^{2+}-dependent regulation of NCX variants in distinct tissues is hampered because the available experimental tools are quite limited in terms of useful mutant design. For example, most mutations in the Ca^{2+} binding sites of CBD1 and CBD2 of intact NCX reduce the affinity of Ca^{2+}-dependent regulation,[13,14,21,22] which limits the use of these mutants in physiological studies. Interestingly, electrophysiological experiments revealed that mutations of either G503 in intact NCX1 or G555 in CALX1.1 (exhibiting an inhibitory response to regulatory Ca^{2+}) nearly completely lack Ca^{2+}-dependent regulation in the cellular system.[33,44] The similar effect in CALX underscores the conserved role of glycine in the linker and the fact that the mutation's effect is not related to the altered binding properties of CBD2 (as it does not bind Ca^{2+} in CALX). In another study, the G503 mutant of NCX1 was used to segregate the Ca^{2+}- and voltage-dependent effects governing NCX regulation in the cellular system.[34] Because our findings revealed that G503 provides the needed flexibility to the linker for dynamic coupling of ligand-induced regulation, G503 mutants could serve as a very instrumental tool for elucidating the contributions of Ca^{2+}-dependent regulation of NCX variants to homeostasis in various cell types.

In summary, we found that the linker's G503 is an obligatory amino acid for facilitating Ca^{2+}-induced tethering of CBDs and slow dissociation of occluded Ca^{2+} from the two-domain regulatory tandem of NCX proteins. Therefore, the G503-controlled flexibility of the linker is required to match local contacts between CBDs, which in turn is mandatory for

dx.doi.org/10.1021/bi300739z | *Biochemistry* XXXX, XXX, XXX−XXX

stabilizing stochastic oscillations of the linker to rigidify CBD movements. This CBD1−CBD2 interface serves as a common module for regulatory coupling in NCX proteins,[29] the dynamic properties of which are auxiliary-aided by an alternative splicing segment located nearby on CBD2 of NCX variants.[16,23]

■ ASSOCIATED CONTENT

Ⓢ Supporting Information

Fitting parameters of Ca^{2+} binding (Table S1) and Ca^{2+} off rates (Table S2) in CBD12 mutants. This material is available free of charge via the Internet at http://pubs.acs.org.

■ AUTHOR INFORMATION

Corresponding Author

*Department of Physiology and Pharmacology, Sackler School of Medicine, Tel-Aviv University, Ramat-Aviv, Tel-Aviv 69978, Israel. Telephone: 972-3-640-9961. Fax: 972-3-640-9113. E-mail: dhanan@post.tau.ac.il.

Funding

This work was partially funded by the Israeli Ministry of Health (Grant 2010-3-6266), the United States-Israeli Binational Science Foundation (Grant 2009-334), and the Israel Science Foundation (Grant 23/10). The support of the Bernstein foundation is highly appreciated. Moshe Giladi is supported by the Clore Scholars Program of the Clore Israel Foundation.

Notes

The authors declare no competing financial interest.

■ ACKNOWLEDGMENTS

We are grateful to Advanced Photon Source scientists Soenke Seifert, Xiaobing Zuo, and Randall Winans for their kind help with the SAXS experiments. We are also thankful to the anonymous reviewers for helpful comments.

■ ABBREVIATIONS

NCX, sodium−calcium exchanger; CBD, calcium binding domain; SAXS, small-angle X-ray scattering; Fluo-3, *N*-[(2-{2-[bis(carboxymethyl)amino]-5-(2,7-dichloro-6-hydroxy-3-oxy-3*H*-xanthen-9-yl)phenoxy}ethoxy)-4-methylphenyl]-*N*-(carboxymethyl)glycine; Quin-2, 2-{[2-bis(carboxymethyl)-amino-5-methylphenoxy]methyl}-6-methoxy-8-bis-(carboxymethyl)aminoquinoline; EDTA, ethylenediaminetetra-acetic acid; SE, standard error.

■ REFERENCES

(1) Wriggers, W., Chakravarty, S., and Jennings, P. A. (2005) Control of protein functional dynamics by peptide linkers. *Biopolymers 80*, 736−746.

(2) Gokhale, R. S., and Khosla, S. (2000) Role of linkers in communication between protein module. *Curr. Opin. Chem. Biol. 4*, 22−27.

(3) George, R. A., and Heringa, J. (2002) An analysis of protein domain linkers: Their classification and role in protein folding. *Protein Eng. 15*, 871−879.

(4) Liu, J., and Nussinov, R. (2010) Molecular dynamics reveal the essential role of linker motions in the function of cullin-RING E3 ligases. *J. Mol. Biol. 396*, 1508−1523.

(5) Piazza, F., and Sanejouand, Y. H. (2009) Long-range energy transfer in proteins. *Phys. Biol. 6*, 046014.

(6) Tsai, C. J., del Sol, A., and Nussinov, R. (2008) Allostery: Absence of a change in shape does not imply that allostery is not at play. *J. Mol. Biol. 378*, 1−11.

(7) Ma, B., Tsai, C.-J., Haliloğlu, T., and Nussinov, R. (2011) Dynamic Allostery: Linkers are not merely flexible. *Structure 19*, 907−917.

(8) Philipson, K. D., and Nicoll, D. A. (2000) Sodium-calcium exchange: A molecular perspective. *Annu. Rev. Physiol. 62*, 111−133.

(9) Blaustein, M. P., and Lederer, W. J. (1999) Sodium/calcium exchange: Its physiological implications. *Physiol. Rev. 79*, 763−854.

(10) Khananshvili, D. (1998) Structure, mechanism and regulation of the cardiac sarcolemma Na^+-Ca^{2+} exchanger. *Mol. Cell. Biol. 23B*, 309−356.

(11) Matsuoka, S., Nicoll, D. A., Reilly, R. F., Hilgemann, D. W., and Philipson, K. D. (1993) Initial localization of regulatory regions of the cardiac sarcolemmal Na^+-Ca^{2+} exchanger. *Proc. Natl. Acad. Sci. U.S.A. 90*, 3870−3874.

(12) Hilge, M., Aelen, J., and Vuister, G. W. (2006) Ca^{2+} regulation in the Na^+/Ca^{2+} exchanger involves two markedly different Ca^{2+} sensors. *Mol. Cell 22*, 15−25.

(13) Nicoll, D. A., Sawaya, M. R., Kwon, S., Cascio, D., Philipson, K. D., and Abramson, J. (2006) The crystal structure of the primary Ca^{2+} sensor of the Na^+/Ca^{2+} exchanger reveals a novel Ca^{2+} binding motif. *J. Biol. Chem. 281*, 21577−21581.

(14) Besserer, G. M., Ottolia, M., Nicoll, D. A., Chaptal, V., Cascio, D., Philipson, K. D., and Abramson, J. (2007) The second Ca^{2+}-binding domain of the Na^+/Ca^{2+} exchanger is essential for regulation: Crystal structures and mutational analysis. *Proc. Natl. Acad. Sci. U.S.A. 104*, 18467−18472.

(15) Kofuji, P., Lederer, W. J., and Schulze, D. H. (1994) Mutually exclusive and cassette exons underlie alternatively spliced isoforms of the Na/Ca exchanger. *J. Biol. Chem. 269*, 5145−5149.

(16) Hilge, M., Aelen, J., Foarce, A., Perrakis, A., and Vuister, G. W. (2009) Ca^{2+} regulation in the Na^+/Ca^{2+} exchanger features a dual electrostatic switch mechanism. *Proc. Natl. Acad. Sci. U.S.A. 106*, 14333−14331.

(17) Liao, J., Li, H., Zeng, W., Sauer, D. B., Belmares, R., and Jiang, Y. (2012) Structural insight into the ion-exchange mechanism of the sodium/calcium exchanger. *Science 335*, 686−690.

(18) Boyman, L., Mikhasenko, H., Hiller, R., and Khananshvili, D. (2009) Kinetic and equilibrium properties of regulatory calcium sensors of NCX1 protein. *J. Biol. Chem. 284*, 6185−6193.

(19) Giladi, M., Boyman, L., Mikhasenko, H., Hiller, R., and Khananshvili, D. (2010) Essential role of the CBD1-CBD2 linker in slow dissociation of Ca^{2+} from the regulatory two-domain tandem of NCX1. *J. Biol. Chem. 285*, 28117−28125.

(20) John, S. A., Ribalet, B., Weiss, J. N., Philipson, K. D., and Ottolia, M. (2011) Ca^{2+}-dependent structural rearrangements within Na^+-Ca^{2+} exchanger dimers. *Proc. Natl. Acad. Sci. U.S.A. 108*, 1699−1704.

(21) Ottolia, M., Nicoll, D. A., and Philipson, K. D. (2009) Roles of two Ca^{2+}-binding domains in regulation of the cardiac Na^+-Ca^{2+} exchanger. *J. Biol. Chem. 284*, 32735−32741.

(22) Ottolia, M., Nicoll, D. A., John, S., and Philipson, K. D. (2010) Interactions between Ca^{2+} binding domains of the Na^+-Ca^{2+} exchanger and secondary regulation. *Channels 4*, 1−4.

(23) Giladi, M., Bohbot, H., Buki, T., Schulze, D. H., Hiller, R., and Khananshvili, D. (2012) Dynamic features of allosteric Ca^{2+} sensor in tissue-specific NCX variants. *Cell Calcium 51*, 478−85.

(24) Boyman, L., Hagen, B. M., Giladi, M., Hiller, R., Lederer, W. J., and Khananshvili, D. (2011) Proton-sensing Ca^{2+} binding domains regulate the cardiac Na^+/Ca^{2+} exchanger. *J. Biol. Chem. 286*, 28811−28820.

(25) Salinas, R. K., Bruschweiler-Li, L., Johnson, E., and Bruschweiler, R. (2011) Ca^{2+} binding alters the interdomain flexibility between the two cytoplasmic calcium-binding domains in the Na^+/Ca^{2+} exchanger. *J. Biol. Chem. 286*, 32123−32131.

(26) Hilgemann, D. W., Matsuoka, S., Nagel, G. A., and Collins, A. (1992) Steady-state and dynamic properties of cardiac sodium-calcium exchange. Sodium-dependent inactivation. *J. Gen. Physiol. 100*, 905−932.

(27) Hilgemann, D. W., Collins, A., and Matsuoka, S. (1992) Steady-state and dynamic properties of cardiac sodium-calcium exchange.

Secondary modulation by cytoplasmic calcium and ATP. *J. Gen. Physiol. 100*, 933−961.
(28) Chaptal, V., Ottolia, M., Mercado-Besserer, G., Nicoll, D. A., Philipson, K. D., and Abramson, J. (2009) Structure and functional analysis of a Ca^{2+} sensor mutant of the Na^+/Ca^{2+} exchanger. *J. Biol. Chem. 284*, 14688−14692.
(29) Giladi, M., Sasson, Y., Fang, X., Hiller, R., Buki, T., Wang, Y. X., Hirsch, J. A., and Khananshvili, D. (2012) A Common Ca^{2+}-Driven Interdomain Module Governs Eukaryotic NCX Regulation. *PLoS One 7*, e39985.
(30) Wu, M., Tong, S., Gonzalez, J., Jayaraman, V., Spudich, J. L., and Zheng, L. (2011) Structural basis of the Ca^{2+} inhibitory mechanism of *Drosophila* Na^+/Ca^{2+} exchanger CALX and its modification by alternative splicing. *Structure 19*, 1509−1517.
(31) Wu, M., Wang, M., Nix, J., Hryshko, L. V., and Zheng, L. (2009) Crystal structure of CBD2 from the *Drosophila* Na^+/Ca^{2+} exchanger: Diversity of Ca^{2+} regulation and its alternative splicing modification. *J. Mol. Biol. 387*, 104−112.
(32) Wu, M., Le, H. D., Wang, M., Yurkov, V., Omelchenko, A., Hnatowich, M., Nix, J., Hryshko, L. V., and Zheng, L. (2010) Crystal structures of progressive Ca^{2+} binding states of the Ca^{2+} sensor Ca^{2+} binding domain 1 (CBD1) from the CALX Na^+/Ca^{2+} exchanger reveal incremental conformational transitions. *J. Biol. Chem. 285*, 2554−2561.
(33) Matsuoka, S., Nicoll, D. A., Hryshko, L. V., Levitsky, D. O., Weiss, J. N., and Philipson, K. D. (1995) Regulation of the cardiac Na^+-Ca^{2+} exchanger by Ca^{2+}. Mutational analysis of the Ca^{2+} binding domain. *J. Gen. Physiol. 105*, 403−420.
(34) Zhang, X. Q., Wang, J., Song, J., Ji, A. M., Chan, T. O., and Cheung, J. Y. (2011) Residues 248−252 and 300−304 of the cardiac Na^+/Ca^{2+} exchanger are involved in its regulation by phospholemman. *Am. J. Physiol. 301*, C833−C840.
(35) Breukels, V., and Vuister, G. W. (2010) Binding of calcium is sensed structurally and dynamically throughout the second calcium-binding domain of the sodium/calcium exchanger. *Proteins 78*, 1813−182.
(36) Flicek, P., Amode, M. R., Barrell, D., Beal, K., Brent, S., Chen, Y., Clapham, P., Coates, G., Fairley, S., Fitzgerald, S., Gordon, L., Hendrix, M., Hourlier, T., Johnson, N., Kahari, A., Keefe, D., Keenan, S., Kinsella, R., Kokocinski, F., Kulesha, E., Larsson, P., Longden, I., McLaren, W., Overduin, B., Pritchard, B., Riat, H. S., Rios, D., Ritchie, G. R., Ruffier, M., Schuster, M., Sobral, D., Spudich, G., Tang, Y. A., Trevanion, S., Vandrovcova, J., Vilella, A. J., White, S., Wilder, S. P., Zadissa, A., Zamora, J., Aken, B. L., Birney, E., Cunningham, F., Dunham, I., Durbin, R., Fernandez-Suarez, X. M., Herrero, J., Hubbard, T. J., Parker, A., Proctor, G., Vogel, J., and Searle, S. M. (2011) Ensembl 2011. *Nucleic Acids Res. 39*, D800−D806.
(37) Thompson, J. D., Gibson, T. J., and Higgins, D. G. (2002) Multiple sequence alignment using ClustalW and ClustalX. *Current Protocols in Bioinformatics*, Chapter 2, Unit 2, p 3, Wiley, New York.
(38) Ashkenazy, H., Erez, E., Martz, E., Pupko, T., and Ben-Tal, N. (2010) ConSurf 2010: Calculating evolutionary conservation in sequence and structure of proteins and nucleic acids. *Nucleic Acids Res. 38*, W529−W533.
(39) Konarev, P. V., Volkov, V. V., Sokolova, A. V., Koch, M. H. J., and Svergun, D. I. (2003) PRIMUS: A Windows-PC based system for small-angle scattering data analysis. *J. Appl. Crystallogr. 36*, 1277−1282.
(40) Svergun, D. I. (1992) Determination of the regularization parameter in indirect-transform methods using perceptual criteria. *J. Appl. Crystallogr. 25*, 495−503.
(41) Svergun, D. I. (1999) Restoring low resolution structure of biological macromolecules from solution scattering using simulated annealing. *Biophys. J. 76*, 2879−2886.
(42) Volkov, V. V., and Svergun, D. I. (2003) Uniqueness of ab-initio shape determination in small-angle scattering. *J. Appl. Crystallogr. 36*, 860−864.
(43) Kozin, M., and Svergun, D. I. (2001) Automated matching of high- and low-resolution structural models. *J. Appl. Crystallogr. 34*, 33−41.
(44) Dyck, C., Maxwell, K., Buchko, J., Trac, M., Omelchenko, A., Hnatowich, M., and Hryshko, L. V. (1998) Structure-function analysis of CALX1.1, a Na^+-Ca^{2+} exchanger from *Drosophila*. Mutagenesis of ionic regulatory sites. *J. Biol. Chem. 273*, 12981−12987.